Pergamon

Chaos, Solitons & Fractals Vol. 10, No. 9, pp. 1473–1489, 1999

0960-0779/99/$ - see front matter

PII: S0960-0779(98)00132-5

Chaos Control by Nonfeedback Methods in the Presence of Noise

M. RAMESH and S. NARAYANAN*

Machine Dynamics Laboratory, Department of Applied Mechanics, Indian Institute of Technology, Madras 600 036, India

(Accepted 5 May 1998)

Abstract—Nonfeedback methods of chaos control are suited for practical applications because of their speed, flexibility, no online monitoring and processing requirements. For applications where none, no real-time, or only highly restricted measurements of the system are available, or where the system behavior is to be altered more drastically, these schemes are quite useful. These methods convert the chaotic motion to *any* arbitrary fixed point or periodic orbit or quasiperiodic orbit. These attributes make them promising for controlling chaotic circuits, fast electro-optical systems, systems in which no parameter is accessible for control, and so on. For possible practical applications of the control methods, the robustness of the methods in the presence of noise is of special interest. The noise can be in the form of external disturbances to the system or in the form of uncertainties due to inexact modelling of the system. In this paper, we make an analysis of the control performance of various nonfeedback methods in controlling the chaotic behavior in the presence of noise in the chaotic system. The various nonfeedback methods considered for the analysis are: addition of (i) constant force, (ii) weak periodic force, (iii) periodic delta-pulses, (iv) rectangular-pulses. The examples considered for this study are the Murali–Lakshmanan–Chua Circuit, and Duffing–Ueda oscillator.

1. INTRODUCTION

Controlling chaos is very important in many circumstances from the point of view of preventing disaster and collapse in a dynamical system. In recent years, after the pioneering work of Ott, Grebogi and Yorke (OGY) [1], controlling chaos has become more and more interesting in academic research and practical applications. Chaos control algorithms can be broadly classified into two categories: feedback and nonfeedback. Feedback methods [1–6] control chaos by *stabilizing* a desired unstable periodic orbit embedded in a chaotic attractor by applying small temporal perturbations to an accessible system parameter. The perturbation required is calculated at every instance and is proportional to the difference between the actual state and the desired state. In the nonfeedback methods [7–11] chaotic motion is *suppressed* by converting the system dynamics to a periodic orbit. In this case, weak periodic perturbations are applied on some control parameters or variables. No knowledge of the fixed points in phase-space is required. Nonfeedback methods of chaos control are suited for practical applications because of their speed, flexibility, no online monitoring and processing requirements. It is also suitable for applications where none, no real-time, or only highly restricted measurements of the system are available, or where the system behavior is to be altered more drastically. Besides we can convert the chaotic motion to *any* periodic orbit. The nonfeedback methods include addition of constant

* Author to whom correspondence is to be adddressed.

force or bias [9], addition of weak periodic parametric perturbation [8], addition of second periodic force [7], addition of weak periodic pulses, entrainment control [10], and addition of quasiperiodic force [11]. Recently, various nonfeedback methods have been briefly discussed in [12] for controlling chaos in the MLC circuit and control by entrainment in the FitzHugh–Nagumo equation.

For possible practical applications of the control methods, the robustness of the methods in the presence of noise is of special interest. The noise can be in the form of external disturbances to the system or in the form of uncertainties due to inexact modelling of the system. Nitsche and Dressler, in their earlier work [2], have investigated the robustness of the feedback control methods, namely, the original method of OGY [1], and the two modified versions [2] of the OGY method, in the presence of measurement noise. Recently, the effect of external noise in the form of a Gaussian white noise with zero mean and standard deviation equal to one has been investigated [13] in the study of generalized synchronization of chaos using symbolic analysis technique.

This paper investigates the control performance of the nonfeedback methods in controlling chaos in the presence of random noise in the system. We have considered the control schemes for two dissipative, non-autonomous systems, viz., Murali–Lakshmanan–Chua (MLC) circuit [9, 12] and Duffing–Ueda oscillator [14]. The noise is introduced into the system equations in the form of a random noise signal given by $\varepsilon\eta$ into the system equations, where ε is a parameter specifying the intensity of the noise and η is a random variable chosen to be uniformly distributed in the interval $[-1, 1]$. The noise is input at each integral step.

This paper is organized as follows: In Section 2, we consider the addition of constant bias or force to MLC equation and Duffing–Ueda equation and investigate the control performance in the presence of random noise in the systems. In Section 3, we study the control performance in the presence of noise in the two systems when the control is effected by the addition of weak periodic force. Section 4 considers the control performance in the presence of noise in the systems when the control is effected by the addition of periodic pulses, and also when periodic short-width rectangular force is applied to the system. Finally, summary and conclusions are given in Section 5.

2. CONTROL PERFORMANCE IN THE PRESENCE OF NOISE WHEN CONTROL IS EFFECTED BY ADDITION OF CONSTANT BIAS OR FORCE TO A CHAOTIC SYSTEM

2.1. MLC Circuit

The MLC circuit shown in Fig. 1 [12] is the simplest dissipative non-autonomous chaotic nonlinear circuit. It consists of a linear capacitor (C), a linear inductor (L), a linear resistor (R) and a nonlinear Chua's diode (N) and an external periodic forcing source. The mathematical model for this circuit is [9]

$$C\frac{dv}{dt} = i_L - g(v) \tag{1}$$

$$L\frac{di_L}{dt} = -Ri_L - v + f\sin(\Omega t) \tag{2}$$

where f is the amplitude, Ω is the frequency of the external periodic signal, v is the voltage and i_L is the current through the inductor and $g(v)$ represents the v–i characteristic of the Chua's diode and is given by [9]

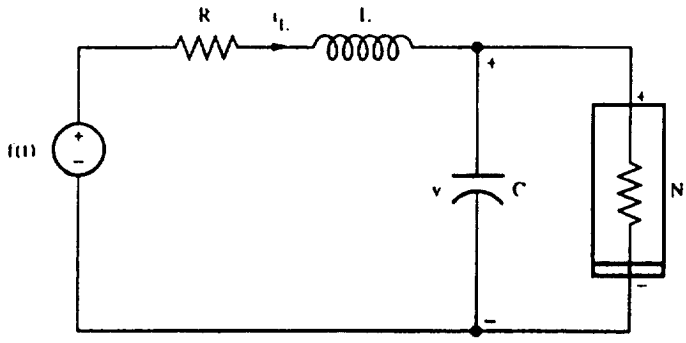

Fig. 1. Circuit diagram of the MLC circuit: $R=1360\ \Omega$, $L=18$ mH, $C=10$ nF and the frequency of the external force $=8890$ Hz.

$$g(v)=G_b v+0.5(G_a-G_b)(|v+B_p|-|v-B_p|) \tag{3}$$

where G_a, G_b and B_p are diode constants. By introducing rescaled variables and parameters, the above equations can be written in dimensionless form as [9]

$$\dot{x}=y-g(x) \tag{4}$$

$$\dot{y}=-\sigma y-\beta x+F\sin(\omega t) \tag{5}$$

where

$$g(x)=bx+0.5(a-b)[|x+1|-|x-1|] \tag{6}$$

and σ, β, a and b are rescaled circuit parameters of eqs. (1–2).

Chaotic behavior is found in the circuit for the specific choice [9] of the parameters $C=10$ nf, $L=18$ mH, $R=1360$ ohm, $G_a=-0.76$ ms, $G_b=-0.41$ ms, $B_p=1.0$ V, external forcing frequency $\Omega/2\pi=8890$ Hz and $f=0.107\ V_{rms}$. For these parameters, the values of β, σ, ω, F, a and b in eqs. (4–6) are calculated as [9] 1.0, 1.015, 0.75, 0.15, −1.02, and −0.55 respectively.

The bifurcation diagram is shown in Fig. 2(a) with F as a bifurcation parameter which shows a period-doubling route to chaos. For the above parameter values, upon numerical integration of eqs. (4–5), a double scroll attractor is found to occur which is shown in Fig. 2(b).

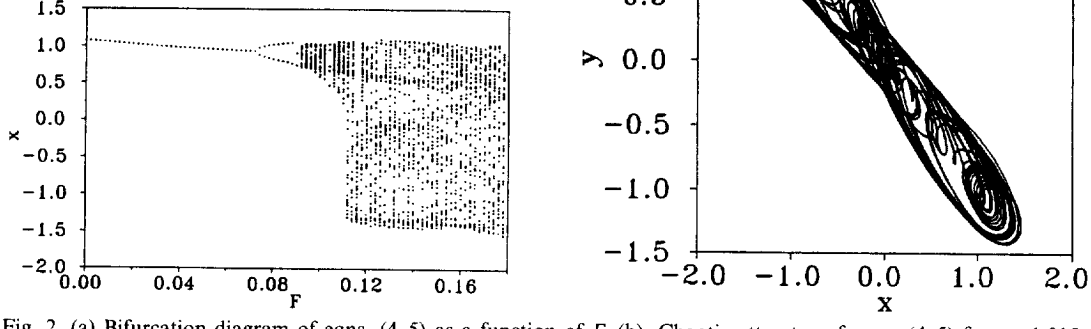

Fig. 2. (a) Bifurcation diagram of eqns. (4–5) as a function of F. (b). Chaotic attractor of eqns. (4–5) for $\sigma=1.015$, $\beta=1.0$, $\omega=0.75$, $F=0.15$, $a=-1.02$, $b=-0.55$.

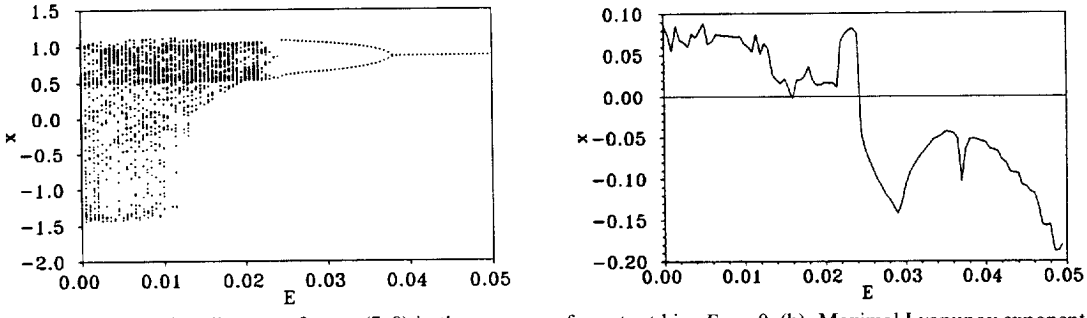

Fig. 3. (a) Bifurcation diagram of eqns. (7–8) in the presence of constant bias E, $\varepsilon=0$. (b). Maximal Lyapunov exponent of eqns. (7–8) in the presence of constant bias E, $\varepsilon=0$.

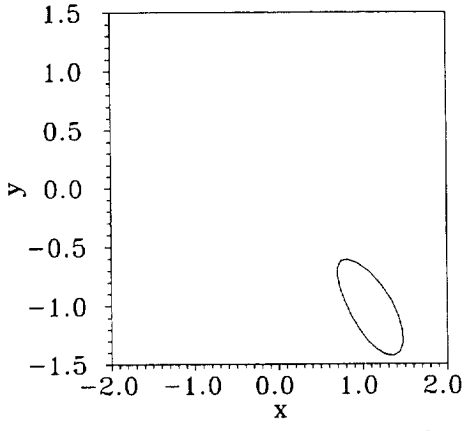

Fig. 3(c). The controlled period-1T attractor of eqns. (7–8) for $E=0.04$, $\varepsilon=0$.

Now a constant bias voltage source and random noise are added in series with the periodic signal $f(t)$. In the presence of the bias element and the random noise, eqs. (4–5) become

$$\dot{x}=y-g(x) \tag{7}$$

$$\dot{y}=-\sigma y-\beta x+F\sin(\omega t)+E+\varepsilon\eta \tag{8}$$

where E is the constant bias. Here $\varepsilon\eta$ is the noise term where ε is a parameter specifying the intensity of the noise and η is a random variable chosen to be uniformly distributed in the interval $[-1, 1]$. Equations (7) and (8) are numerically integrated using the fourth-order Runge–Kutta method with a time step of $\Delta t=T/100$, where $T=2\pi/\omega$. Figure 3(a) shows the bifurcation diagram of eqs. (7–8) with E as the bifurcation parameter and without noise in the system ($\varepsilon=0$). It shows the suppression of chaos by inverse period-doubling bifurcation. Figure 3(b) shows the corresponding maximal Lyapunov exponent spectrum. Periodic behavior is found for $E\geqslant 0.023$. The controlled period-1T orbit for $E=0.04$ and without noise is shown in the x–y phase plane in Fig. 3(c).

The control performance in the presence of noise is studied for $E=0.04$ by varying the noise intensity. The noise is added at every time step from time $t=0$. The control is activated at 200$^{\text{th}}$ drive cycle. The Poincaré points of x at each drive cycle is plotted for different noise intensities

in Fig. 4. After the control is activated, if the deviation of the points in the Poincaré section in the presence of noise in the system from the points in the Poincaré section without noise in the system exceeds a radius of $\zeta = 0.5$, the system is assumed to be out of control. This criterion for robustness of the control methods in the presence of noise has been followed throughout this paper. Thus for a noise intensity $\varepsilon \geqslant 0.2$ the MLC system loses control when the control is effected by the addition of constant bias as shown in Fig. 4(i).

2.2. *Duffing–Ueda oscillator*

The equation of motion for a Duffing–Ueda oscillator is given by [14]

$$\ddot{y} = \alpha \dot{y} + y^3 + A\cos(\omega t) \tag{9}$$

In state space form eqn (9) can be written as

$$\dot{x}_1 = x_2 \tag{10}$$

$$\dot{x}_2 = -\alpha x_2 - x_1^3 + A\cos(\omega t) \tag{11}$$

where $\alpha = 0.1$ and $\omega = 1.0$. The bifurcation diagram of this model is shown in Fig. 5 with A as a bifurcation parameter. We consider the case of $A = 11.5$ for which the chaotic attractor is shown in Fig. 6.

Now a constant force and random noise term are added to eqn (11) to study the influence of noise on the control performance. Thus eqns. (10–11) become

$$\dot{x}_1 = x_2 \tag{12}$$

$$\dot{x}_2 = -\alpha x_2 - x_1^3 + A\cos(\omega t) + F + \varepsilon\eta \tag{13}$$

where F is the constant forcing term and $\varepsilon\eta$ is the noise term where ε is a parameter specifying the intensity of the noise and η is a random variable chosen to be uniformly distributed in the interval $[-1, 1]$.

Equations (12) and (13) are numerically integrated using fourth-order Runge–Kutta method with a time step of $\Delta t = T/200$, where $T = 2\pi/\omega$. Bifurcation diagram of eqns. (12) and (13) with F as a bifurcation parameter and $\varepsilon = 0$ is shown in Fig. 7. Periodic motions are found to exist for $2.1 \leqslant F \leqslant 2.52$ and $F \geqslant 3.1$. The controlled period-1T orbit for $F = 4.0$ and $\varepsilon = 0$ is shown in Fig. 8. We now add noise to the system from time $t = 0$ with different values of noise intensity ε ranging from 0.0 to 0.5. The control is activated at 200$^{\text{th}}$ drive cycle. The plot of Poincaré points are shown for the variable x_1 with different values of noise intensity ε for 500 drive cycles in Fig. 9. It is found that the control is lost ($\zeta > 0.5$) for noise intensity $\varepsilon \geqslant 0.5$.

3. ADDITION OF WEAK-PERIODIC FORCE AND INFLUENCE OF RANDOM NOISE

3.1. *MLC Circuit*

With the addition of a second weak-periodic force and random noise term the MLC circuit eqns. (4–5) become

$$\dot{x} = y - g(x) \tag{14}$$

$$\dot{y} = -\sigma y - \beta x + F\sin(\omega t) + F_2\sin(\omega_2 t) + \varepsilon\eta \tag{15}$$

where $F_2\sin(\omega_2 t)$ is the weak-periodic force and $\varepsilon\eta$ is the random noise term where ε is a parameter specifying the intensity of the noise and η is a random variable chosen to be uniformly distributed

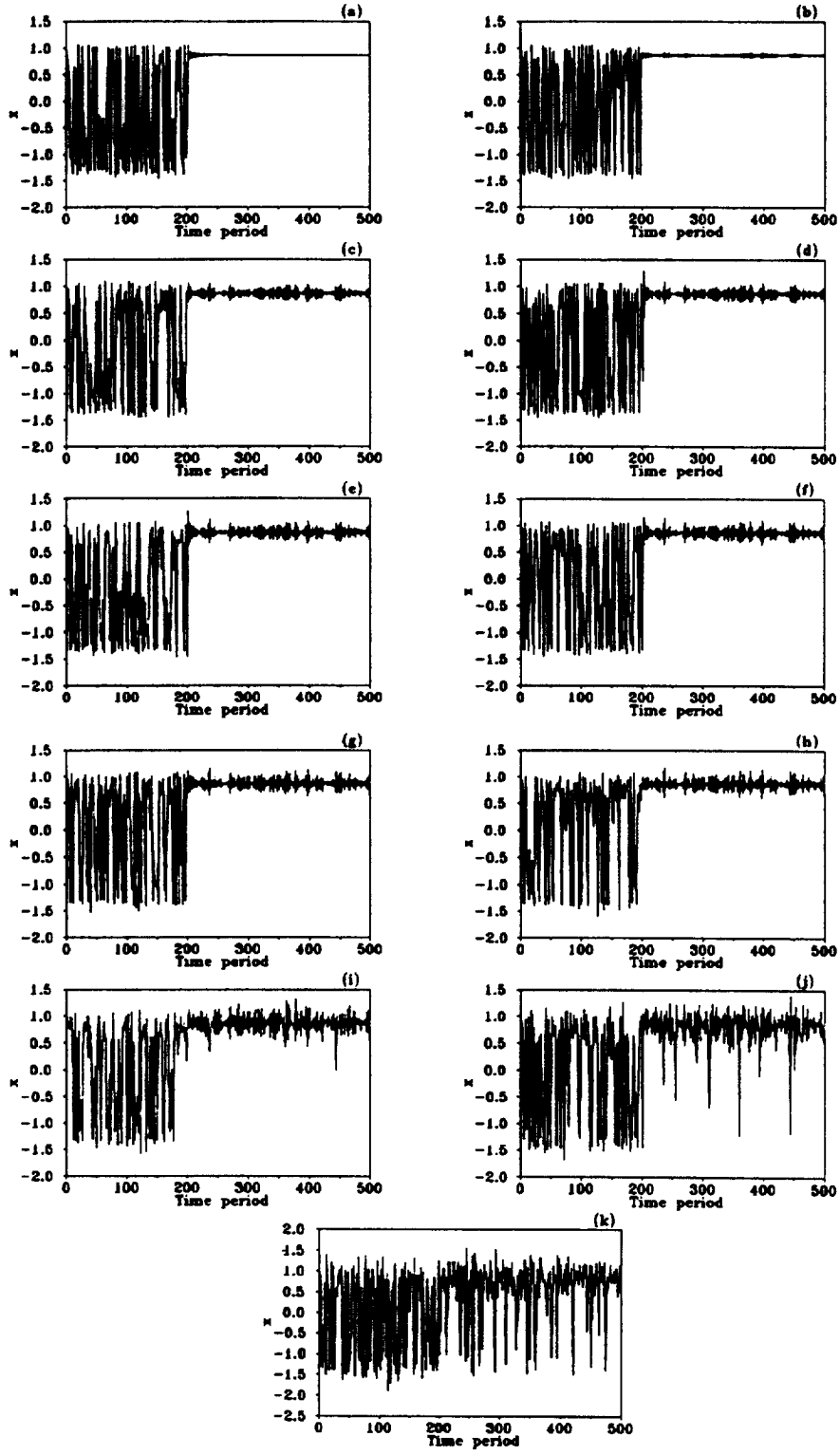

Fig. 4. Poincaré points of x of eqns. (7–8) for $E=0.04$ (a) without noise; and with noise of intensity (b) 0.01, (c) 0.05, (d) 0.06, (e) 0.07, (f) 0.08, (g) 0.09, (h) 0.1, (i) 0.2, (j) 0.3, (k) 0.5. The control is switched on at time period $=200$.

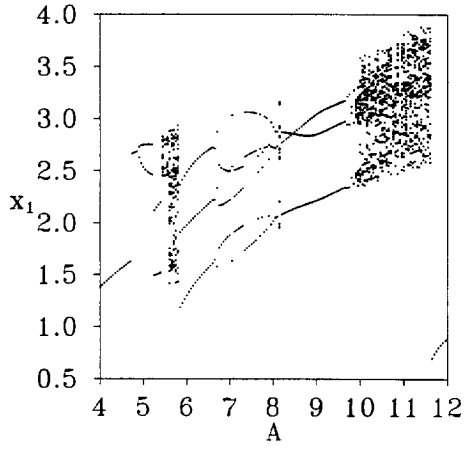

Fig. 5. Bifurcation diagram of eqns. (10) and (11) with A as a bifurcation parameter ($\alpha=0.1$, $\omega=1.0$).

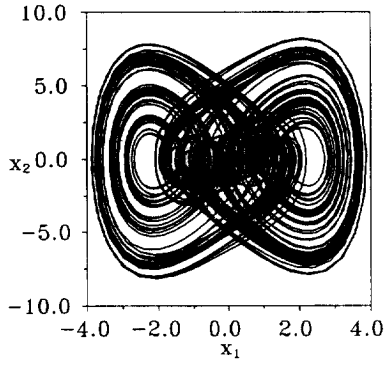

Fig. 6. Chaotic attractor of eqns. (10) and (11) for $\alpha=0.1$, $\omega=1.0$ and $A=11.5$.

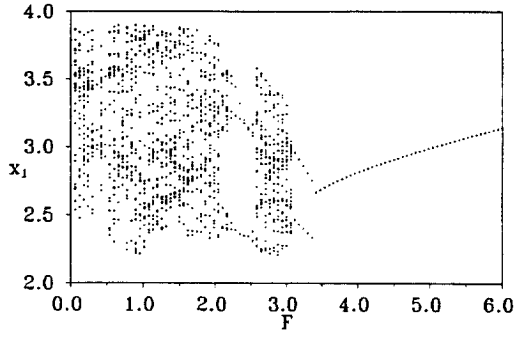

Fig. 7. Bifurcation diagram of eqns. (12-13) in the presence of constant force F ($\varepsilon=0$).

in the interval $[-1, 1]$. For $\sigma=1.015$, $\beta=1.0$, $F=0.15$, $\omega=0.75$, $\omega_2=0.75$, $a=-1.02$, $b=-0.55$ and $\varepsilon=0$, the bifurcation diagram is shown in Fig. 10(a) with F_2 as the bifurcation parameter. The corresponding maximal Lyapunov spectrum is shown in Fig. 10(b).

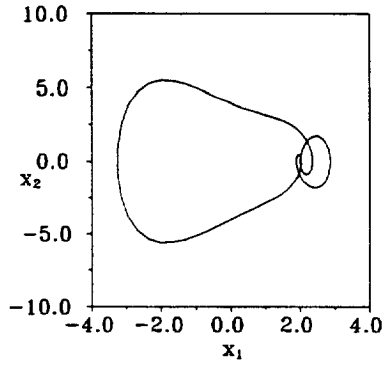

Fig. 8. The controlled period-1T orbit of eqns. (12–13) for F = 4.0 and $\varepsilon = 0$.

Periodic behavior with period-3T is observed for $F_2 \geqslant 0.03$. The controlled period-3T attractor for $F_2 = 0.06$ is shown in Fig. 10(c).

Random noise is added to the system from time $t = 0$ with different noise intensity ε. The control is activated at the 200th drive cycle. The plot of Poincaré points of the dynamical variable x at each drive cycle is shown in Fig. 11 for 500 drive cycles with noise intensity ranging from 0.0 to 0.1. The control is found to be lost ($\zeta > 0.5$) for noise intensity of $\varepsilon > 0.07$ as seen in Fig. 11(f).

3.2. *Duffing–Ueda Oscillator*

In the presence of a second weak-periodic force and random noise term the Duffing–Ueda eqns. (10) and (11) become

$$\dot{x}_1 = x_2 \tag{16}$$

$$\dot{x}_2 = -\alpha x_2 - x_1^3 + A\cos(\omega t) + A_c\cos(\omega_c t) + \varepsilon\eta \tag{17}$$

where $A_c \cos(\omega_c t)$ is the weak-periodic control force and $\varepsilon\eta$ is the random noise term where ε is a parameter specifying the intensity of the noise and η is a random variable chosen to be uniformly distributed in the interval $[-1, 1]$. For $\alpha = 0.1$, $\omega = 1$, $A = 11.5$, $\omega_c = 3.0$, $\varepsilon = 0$ the bifurcation diagram of eqns. (16) and (17) with A_c as the bifurcation parameter is shown in Fig. 12(a). Periodic motions are found for $0.2 \leqslant A_c \leqslant 0.9$ and $1.06 \leqslant A_c \leqslant 1.43$ for $\omega_c = 3.0$. The controlled period-2T attractor for $A_c = 1.2$, $\varepsilon = 0$ and $\omega_c = 3.0$ is shown in Fig. 12(b). Here $T = 2\pi/\omega$.

Now the control performance is investigated by adding noise of different intensity from time $t = 0$. Equations (16) and (17) are numerically integrated and the plot of Poincaré points of x_1 is shown in Fig. 13 for different intensity of noise for $A_c = 1.2$ and $\omega_c = 3.0$. The control is activated from the 200th drive cycle. The control is lost ($\zeta > 0.5$) for noise intensity $\varepsilon \geqslant 0.2$ as can be seen in Fig. 13(e).

4. ADDITION OF WEAK PERIODIC DELTA-PULSES, RECTANGULAR PULSES AND INFLUENCE OF RANDOM NOISE

4.1. *Addition of weak periodic delta-pulses and influence of random noise in MLC circuit*

In this case the external control perturbations are applied at discrete times only. With the addition of delta-pulses and random noise term eqns. (4) and (5) become

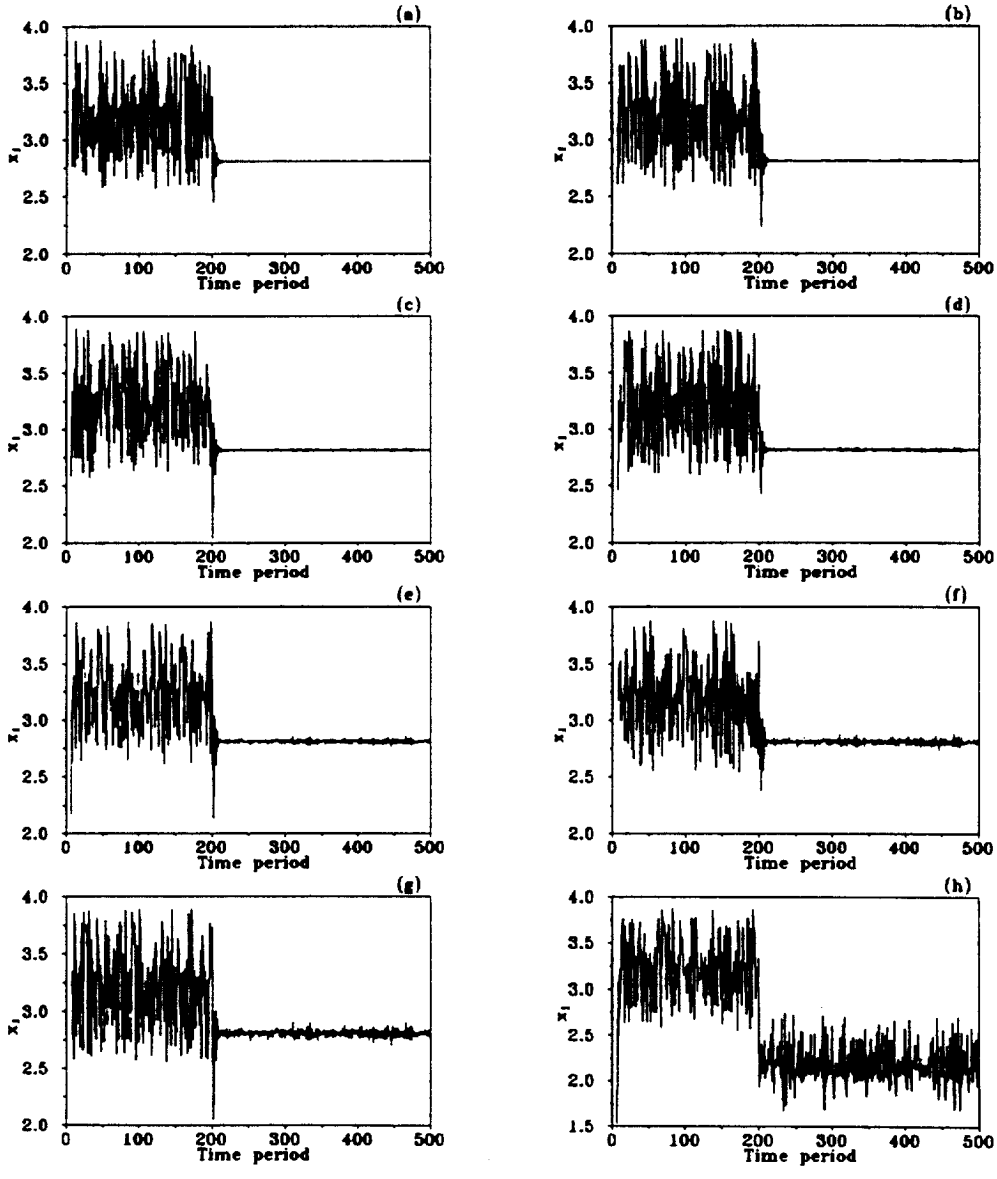

Fig. 9. Poincaré points of x_1 of eqns. (12–13) for $F=4.0$ (a) without noise; and with noise of intensity (b) 0.05, (c) 0.06, (d) 0.1, (e) 0.2, (f) 0.3, (g) 0.4, (h) 0.5. The control is switched on at time period $=200$.

$$\dot{x}=y-g(x) \tag{18}$$

$$\dot{y}=-\sigma y-\beta x+F\sin(\omega t)+\alpha\sum_{n=1}^{\infty}\delta(t-n\tau T)+\varepsilon\eta \tag{19}$$

where $\varepsilon\eta$ is the random noise term, ε is a parameter specifying the intensity of the noise and η is a random variable chosen to be uniformly distributed in the interval $[-1, 1]$. The added force is nonzero only at times $t=n\tau T$, $n=1,2,.$ where $T=2\pi/\omega$. The effect of the force is to shift (x, y) to $(x, y+\alpha)$ at $t=n\tau T$. Chaotic motion is observed in eqns. (18) and (19) for $\sigma=1.015$, $\beta=1.0$, $a=$

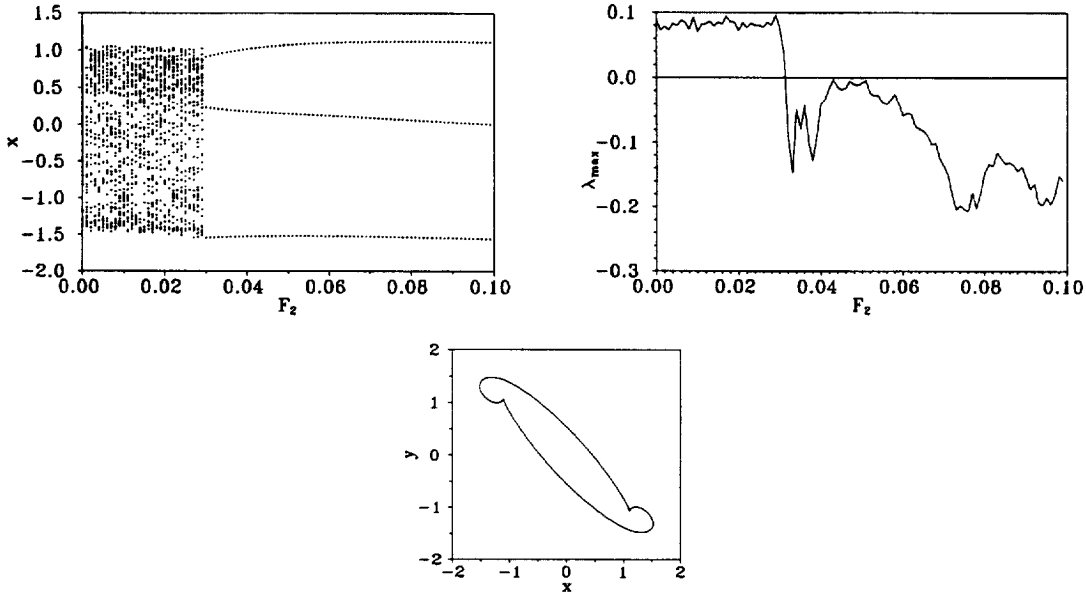

Fig. 10. (a) Bifurcation diagram of eqns. (14) and (15) in the presence of weak periodic force for $\sigma=1.015$, $\beta=1.0$, $F=0.15$, $\omega=0.75$, $\omega_2=0.75$, $a=-1.02$, $b=-0.55$ and $\varepsilon=0$. (b). Maximal Lyapunov exponent spectrum of eqns. (14) and (15) in the presence of weak periodic force for $\sigma=1.015$, $\beta=1.0$, $F=0.15$, $\omega=0.75$, $\omega_2=0.75$, $a=-1.02$, $b=-0.55$ and $\varepsilon=0$. (c). The controlled period-3T attractor of eqns. (14) and (15) for $F_2=0.06$, $\varepsilon=0$.

-1.02, $b=-0.55$, $\omega=0.75$ and $F=0.1$ in the absence of the δ-force and random noise. Fixing τ at 0.25, the bifurcation diagram of eqns. (18) and (19) are obtained as a function of α without noise ($\varepsilon=0$) as shown in Fig. 14(a). With $\tau=0.25$, periodic motions are observed for $\alpha\geqslant 0.08$. The controlled period-$2T$ attractor for $\alpha=0.15$, $\tau=0.25$, $\varepsilon=0$, is shown in Fig. 14(b) in the x–y phase-plane.

Random noise is added as shown in eqns. (18) and (19) from time $t=0$ at every time step and the numerical integration is performed. For different values of noise intensity ε, the Poincaré points of the dynamical variable x are plotted for 500 drive cycles as shown in Fig. 15. The control is activated at the 200$^{\text{th}}$ drive cycle. The system loses control ($\zeta>0.5$) for noise intensity $\varepsilon>0.02$ as seen in Fig. 15(e).

4.2. *Addition of weak periodic delta-pulses and influence of random noise in Duffing–Ueda oscillator*

No effective chaos control is observed for $\alpha<12.0$ for $0.005\leqslant\tau\leqslant 1.0$.

4.3. *Addition of periodic rectangular-pulses and influence of random noise in MLC circuit*

Replacing the delta function force in eqns. (18) and (19) by a rectangular force of short width $h(t)$, we get

$$\dot{x}=y-g(x) \tag{20}$$

$$\dot{y}=-\sigma y-\beta x+F\sin(\omega t)+h(t)+\varepsilon\eta \tag{21}$$

where $h(t)=\alpha$, for $0\leqslant t\leqslant 0.02T$, $0.48T\leqslant t\leqslant 0.52T$ and $0.98T\leqslant t\leqslant T$, with t mod T. Otherwise

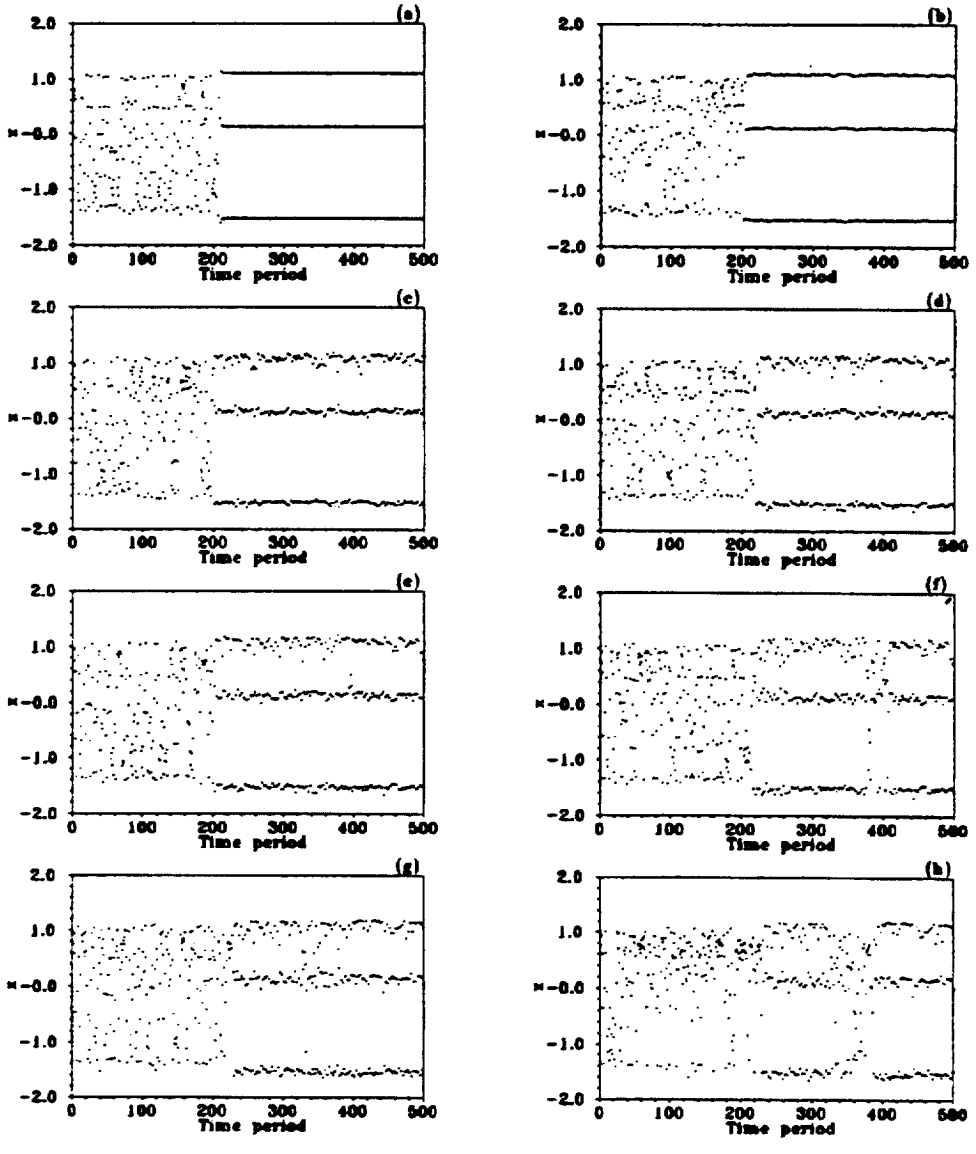

Fig. 11. Poincaré points of x of eqns. (14) and (15) for $F_2=0.06$ (a) without noise, and with noise of intensity (b) 0.01, (c) 0.05, (d) 0.06, (e) 0.07, (f) 0.08, (g) 0.09, (h) 0.1. The control is switched on at time period $=200$.

$h(t)=0$. $\varepsilon\eta$ is the random noise term where ε is a parameter specifying the intensity of the noise and η is a random variable chosen to be uniformly distributed in the interval $[-1, 1]$.

For $\sigma=1.015$, $\beta=1.0$, $a=-1.02$, $b=-0.55$, $\omega=0.75$, $F=0.1$, $\varepsilon=0$, the bifurcation diagram of eqns. (20–21) are plotted as a function of α as shown in Fig. 16(a). Periodic motion is found to occur for $\alpha\geqslant 0.025$. The controlled period-$2T$ attractor for $\alpha=0.2$, $\varepsilon=0$, is shown in Fig. 16(b).

The Poincaré points of the variable x are plotted for different intensities of noise which is added to the system from time $t=0$. The control is activated at the 1500$^{\text{th}}$ drive cycle. Figure 17 shows the Poincaré plots for 2500 drive cycles. The system loses control ($\zeta>0.5$) for noise intensity $\varepsilon\geqslant 0.03$ as seen in Fig. 17(e).

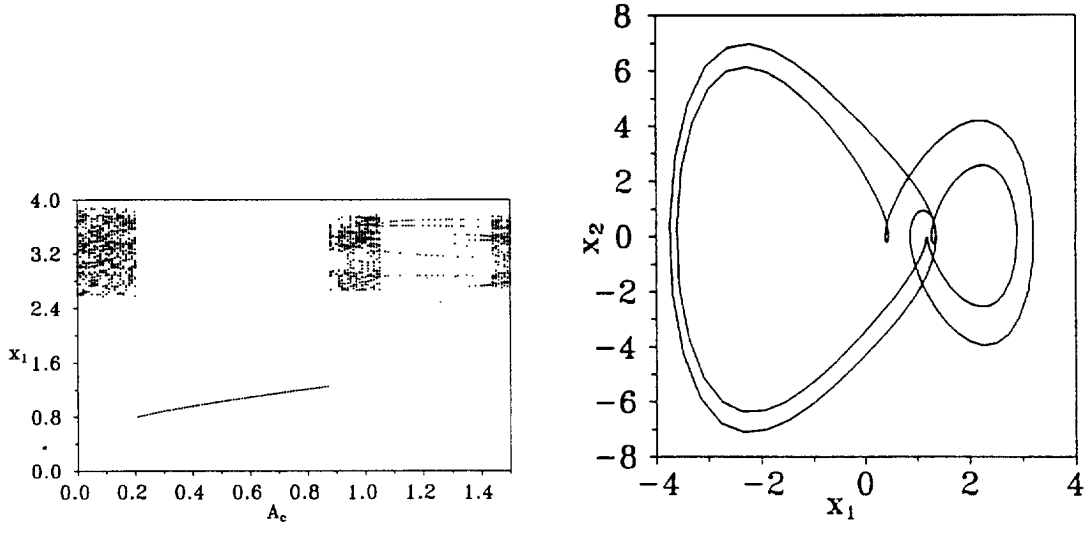

Fig. 12. (a) Bifurcation diagram of eqns. (16) and (17) with A_c as the bifurcation parameter for $\alpha=0.1$, $\omega=1$, $A=11.5$, $\omega_c=3.0$, $\varepsilon=0$. (b). The controlled period-2T attractor of eqns. (16) and (17) for $\alpha=0.1$, $\omega=1$, $A=11.5$, $A_c=1.2$, $\omega_c=3.0$, $\varepsilon=0$.

4.4. Addition of weak periodic rectangular-pulses and influence of random noise in Duffing-Ueda oscillator

In the presence of rectangular pulses and random noise eqns. (10) and (11) become

$$\dot{x}_1 = x_2 \tag{22}$$

$$\dot{x} = -\alpha x_2 - x_1^3 + A\cos(\omega t) + h(t) + \varepsilon\eta \tag{23}$$

where $h(t)=\beta$, for $0 \leqslant t \leqslant 0.02T$, $0.48T \leqslant t \leqslant 0.52T$ and $0.98T \leqslant t \leqslant T$, with t mod T. Otherwise $h(t)=0$. $\varepsilon\eta$ is the random noise term where ε is a parameter specifying the intensity of the noise and η is a random variable chosen to be uniformly distributed in the interval $[-1, 1]$.

For $\alpha=0.1$, $A=11.5$, $\omega=1.0$, $\varepsilon=0$, the bifurcation diagram of eqns. (22) and (23) are obtained as a function of β as shown in Fig. 18(a). The controlled period-1T attractor of Duffing–Ueda eqns. (22) and (23) in the presence of rectangular pulses for $\beta=11.0$ is shown in Fig. 18(b).

By adding the random noise term with different intensities from time $t=0$ and numerically integrating eqs. (22) and (23) we get the Poincaré plots of the dynamical variable x_1 as shown in Fig. 19. Here the control is activated from the 100$^{\text{th}}$ drive cycle. Long control transients are observed for noise intensities of 0.03, 0.05, 0.09 and 0.1. The control is lost ($\zeta > 0.5$) for $\varepsilon \geqslant 0.2$.

5. CONCLUSIONS

In this paper, we have investigated the effectiveness of the various nonfeedback methods in controlling noisy chaotic systems. For illustration purpose, we have considered a chaotic nonlinear electrical circuit, viz., MLC circuit and a chaotic nonlinear mechanical oscillator, viz., Duffing–Ueda oscillator. It is found that the constant force method is more robust in controlling the two noisy chaotic systems considered when compared to the other three methods of control.

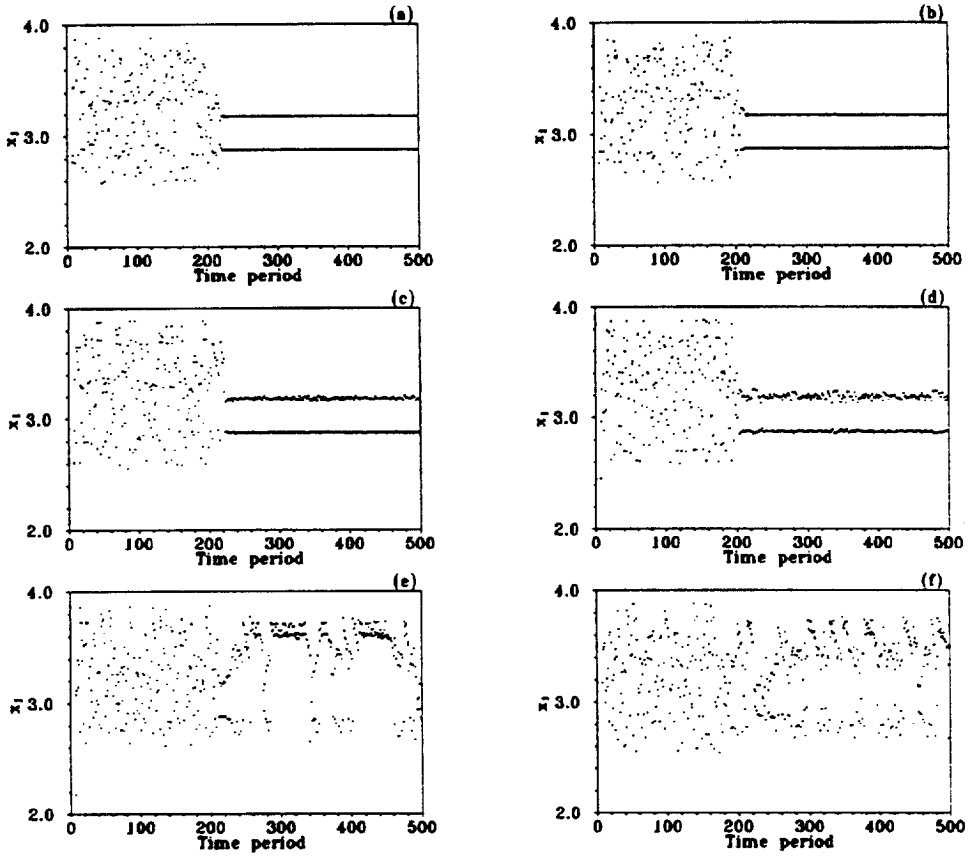

Fig. 13. Poincare points of x_i of eqns. (16) and (17) for $A_c=1.2$, $\omega_c=3.0$ (a) without noise, and with noise of intensity (b) 0.01, (c) 0.05, (d) 0.1, (e) 0.02, (f) 0.3. The control is switched on at time period $=200$.

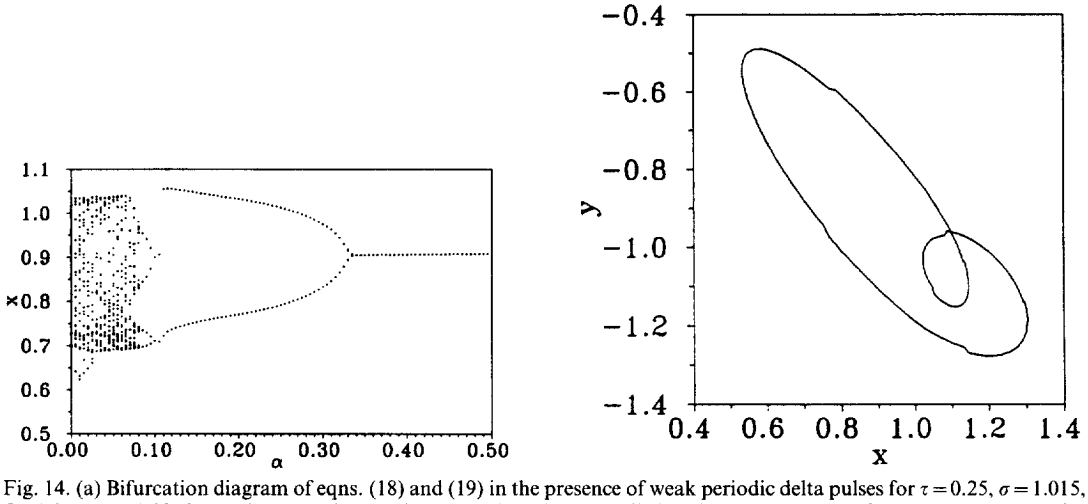

Fig. 14. (a) Bifurcation diagram of eqns. (18) and (19) in the presence of weak periodic delta pulses for $\tau=0.25$, $\sigma=1.015$, $\beta=1.0$, $a=-1.02$, $b=-0.55$, $\omega=0.75$ and $F=0.1$. (b). The controlled period-2T attractor of eqns. (18) and (19) for $\alpha=0.15$, $\tau=0.25$, $\varepsilon=0$.

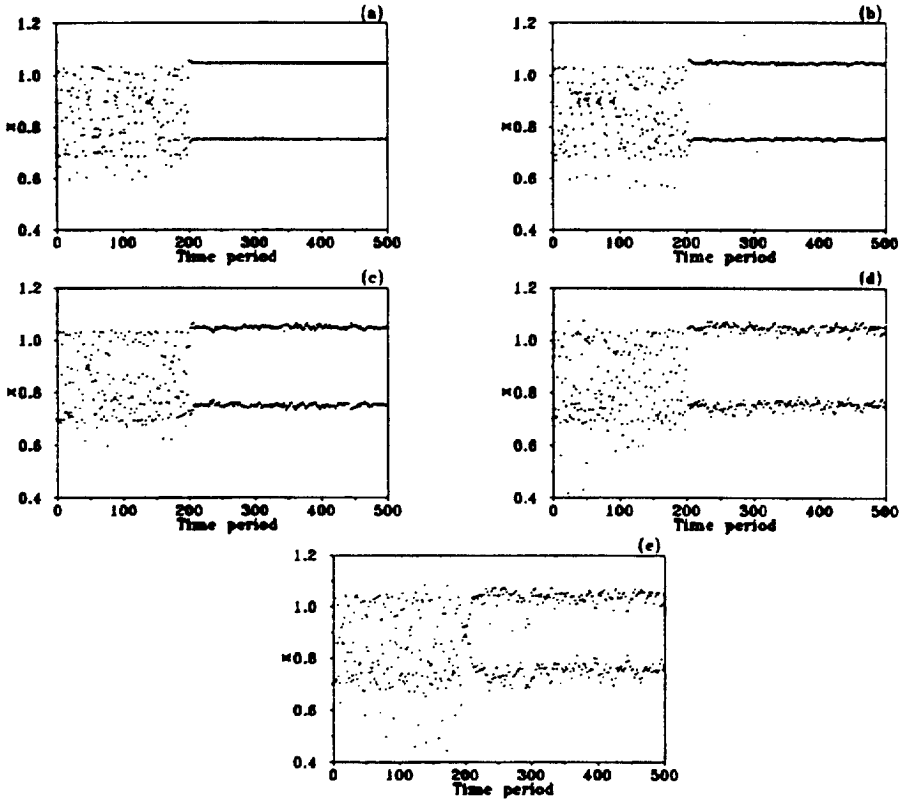

Fig. 15. Poincare points of x of eqns. (18) and (19) for $\alpha=0.15$, $\tau=0.25$ (a) without noise, and with noise of intensity (b) 5.0×10^{-3}, (c) 0.01, (d) 0.02, (e) 0.03. The control is switched on at time period $=200$.

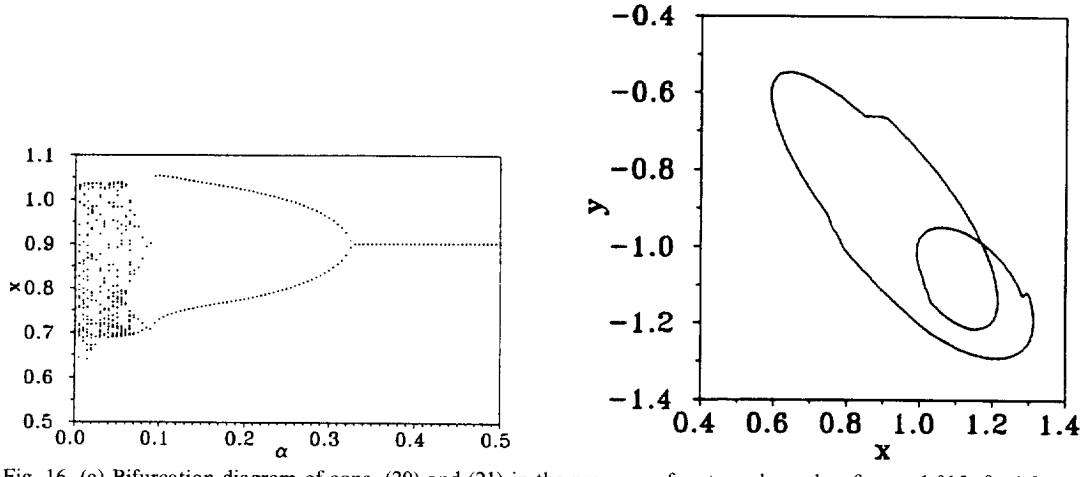

Fig. 16. (a) Bifurcation diagram of eqns. (20) and (21) in the presence of rectangular pulses for $\sigma=1.015$, $\beta=1.0$, $a=-1.02$, $b=-0.55$, $\omega=0.75$, $F=0.1$, $\varepsilon=0$ with α as the bifurcation parameter. (b). Controlled period-$2T$ attractor of the MLC circuit with addition of rectangular force for $\alpha=0.2$, $\varepsilon=0$.

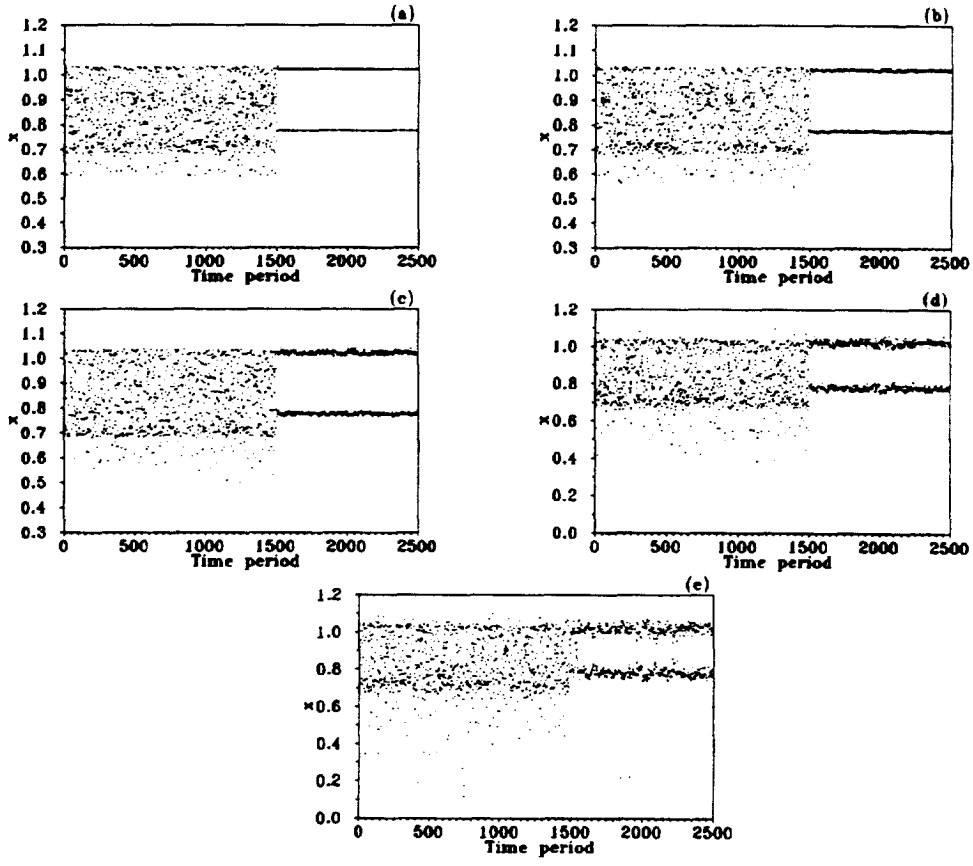

Fig. 17. Poincaré points of x of the MLC circuit with rectangular force ($\alpha = 0.2$) (a) without noise, and with noise of intensity (b) 0.005, (c) 0.01, (d) 0.02, (e) 0.03. The control is switched on at 1500th drive cycle.

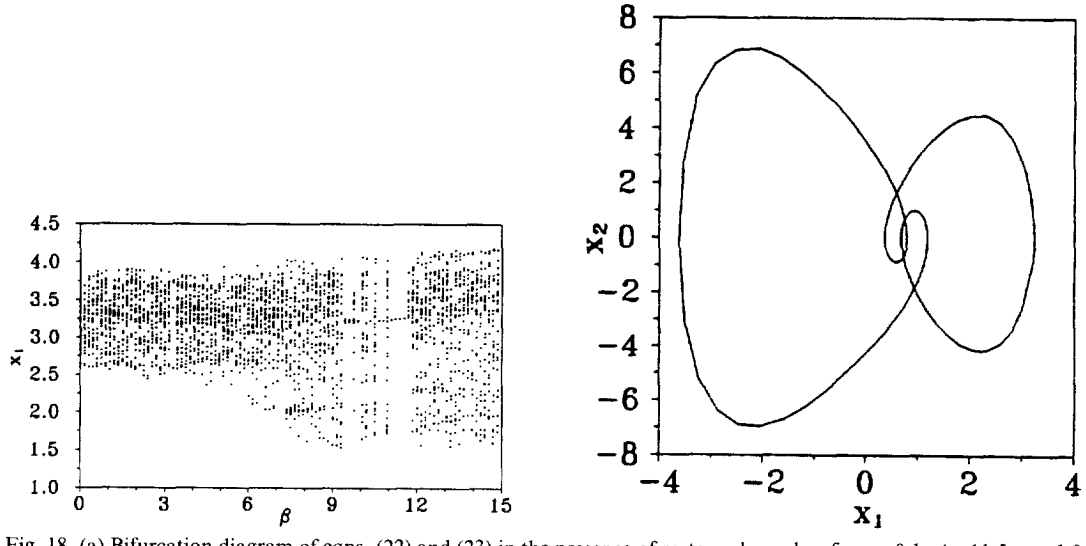

Fig. 18. (a) Bifurcation diagram of eqns. (22) and (23) in the presence of rectangular pulses for $\alpha = 0.1$, $A = 11.5$, $\omega = 1.0$, $\varepsilon = 0$ with β as the bifurcation parameter. (b). The controlled period-1T attractor of eqns. (22) and (23) in the presence of rectangular pulses for $\beta = 11.0$, $\varepsilon = 0$.

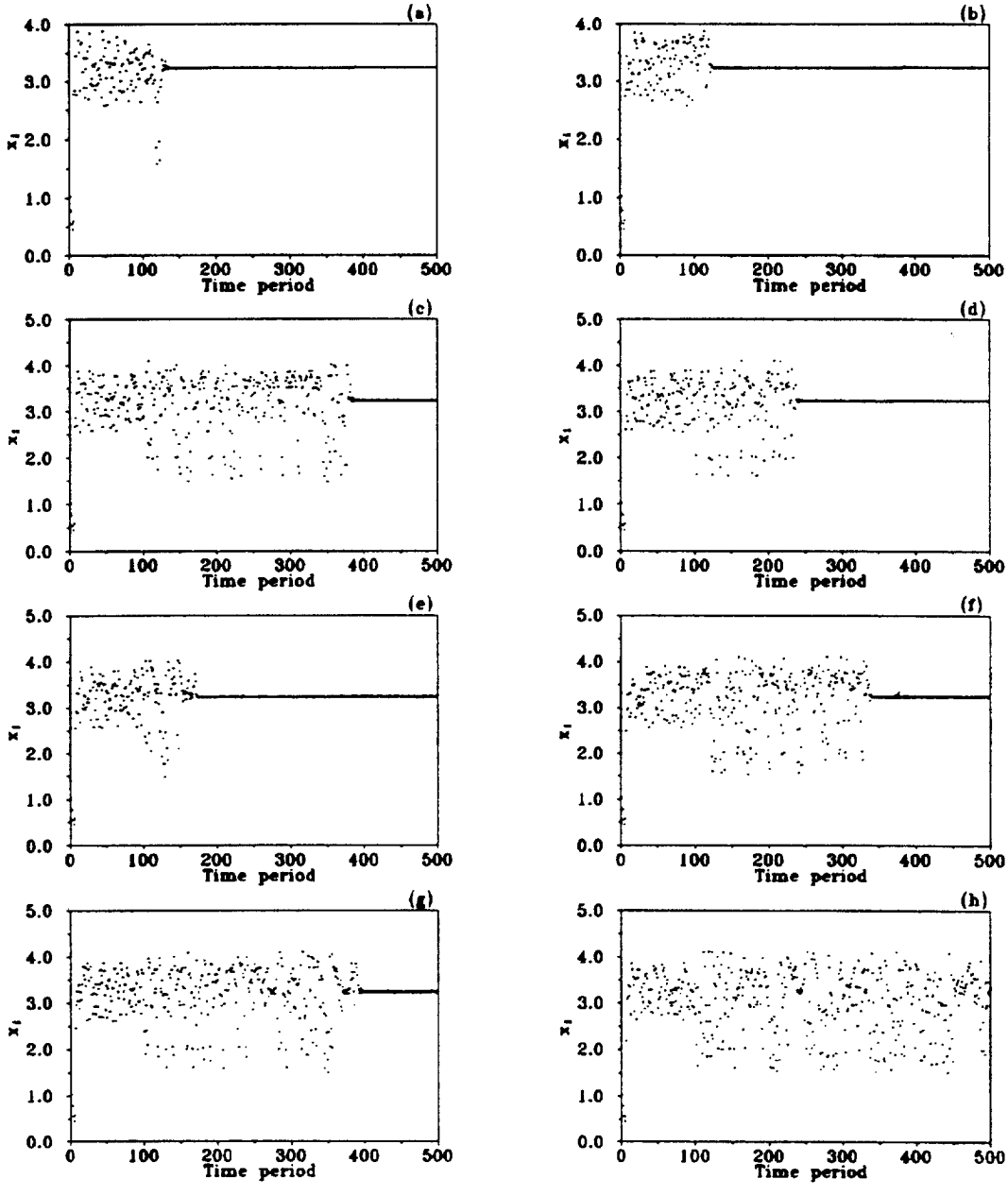

Fig. 19. Poincaré points of x_i of Duffing–Ueda oscillator with rectangular pulse ($\beta = 11.0$) (a) without noise, and with noise of intensity (b) 0.01, (c) 0.03, (d) 0.05, (e) 0.07, (f) 0.09, (g) 0.1, (h) 0.2. The control is switched on at time period = 100.

Table 1. Comparison of the noise tolerance of the nonfeedback methods for controlling chaos in the MLC circuit and the Duffing–Ueda oscillator

		Periodic motion		Noise tolerance	
Control Method	Controller	MLC	Duff-Ueda	MLC	Duff-Ueda
Constant force	$C(t)=C_0=$constant	$C_0 \geqslant 0.023$	$2.1 \leqslant C_0 \leqslant 2.52$ and $C_0 \geqslant 3.1$	$\varepsilon < 0.2$	$\varepsilon < 0.5$
Weak periodic force	$C(t)=\eta \sin(\Omega t)$	$\eta \geqslant 0.03$ ($\Omega = 0.75$)	$0.2 \leqslant \eta \leqslant 0.9$ and $1.06 \leqslant \eta \leqslant 1.43$ ($\Omega = 3.0$)	$\varepsilon < 0.08$	$\varepsilon < 0.2$
Periodic delta pulses	$C(t)=\alpha\Sigma_{n=1}^{\infty}\delta(t-n\tau T)$	$\alpha \geqslant 0.08$ $\tau = 0.25$ $F = 0.1$	No control for values of α upto 15.0	$\varepsilon < 0.03$	—
Short-width rectangular pulses	$C(t)=\alpha$; $0 \leqslant t \leqslant 0.02T$, $0.48T \leqslant t \leqslant 0.52T$ and $0.98T \leqslant t \leqslant T$. $=0$; otherwise.	$\alpha \geqslant 0.025$	$9.45 \leqslant \alpha \leqslant 9.9$; $10.35 \leqslant \alpha \leqslant 10.45$; $10.65 \leqslant \alpha \leqslant 10.9$ and $11.1 \leqslant \alpha \leqslant 11.7$	$\varepsilon < 0.03$	$\varepsilon < 0.2$

For the case of the MLC circuit, the addition of periodic delta pulses or the rectangular pulses are equally effective with respect to each other in controlling chaos in the presence of noise in the circuit but less robust compared to the constant force method. Also, for the case of MLC circuit, control by the addition of weak periodic force is less robust to noise than constant force method and more robust than delta pulses or rectangular force addition. Addition of delta pulses is not found to be very effective in controlling chaotic Duffing–Ueda oscillator, even in the absence of noise. Long control transients are observed for some noise intensities, in chaotic Duffing–Ueda oscillator, with the addition of rectangular force. The robustness of the nonfeedback control methods in the presence of random noise in the two systems considered are shown in Table 1.

REFERENCES

1. Ott, E., Grebogi, C., Yorke, J., Controlling chaos . *Phys. Rev. Lett.*, 1990, **64,** 1196–1199.
2. Dressler, U., Nitsche, G., Controlling chaos using time delay coordinates. *Phys. Rev. Lett.*, 1992, **68,** 1–4.
3. Singer, J., Wang, Y. Z., Bau, H. H., Controlling a chaotic system. *Phys. Rev. Lett.*, 1991, **66,** 1123–1125.
4. Pyragas, K., Continuous control of chaos by self-controlling feedback. *Phys. Lett. A.*, 1992, **170,** 421–428.
5. Sinha, S., Ramaswamy, R., Rao , S. J., Adaptive control in nonlinear dynamics. *Phys. D*, 1990, **43,** 118–128.
6. Chen, G., Dong, X., On feedback control of chaotic dynamic systems. *Int. J. Bifurcation and Chaos*, 1992, **2,** 407–411.
7. Braiman, Y., Goldhirsch, I., Taming chaotic dynamics with weak periodic perturbations. *Phys. Rev. Lett.*, 1991, **66,** 2545–2548.
8. Lima, R., Pettini, M., Suppression of chaos by resonant parametric perturbations. *Phys. Rev. A.*, 1990, **41,** 726–733.
9. Murali, K., Lakshmanan, M., Chua, L. O., Controlling and synchronization of chaos in the simplest dissipative non-autonomous circuit. *Int. J. Bifurcation and Chaos*, 1995, **5,** 563–571.
10. Jackson, E. A., Controls of dynamic flows with attractors. *Phys. Rev. A*, 1991, **44,** 4839–4853.
11. Kapitaniak, T., The loss of chaos in a quasiperiodically-forced nonlinear oscillator. *Int. J. Bifurcation and Chaos*, 1991, **1,** 357–362.
12. Rajasekar, S., Murali, K., Lakshmanan, M., Control of chaos by nonfeedback methods in a simple electronic circuit system and the FitzHugh–Nagumo equation. *Chaos, Solitons and Fractals*, 1997, **8,** 1545–1558.
13. Liu, Z., Chen, S., Symbolic analysis of generalized synchronization of chaos. *Physical Review E*, 1997, **56,** 7297–7300.
14. Ueda, Y., Random phenomena resulting from nonlinearity in the system described by Duffing's equation. *Int. J. Non-Linear Mech.*, 1985, **20,** 481–491.